PCCP

Accepted Manuscript

ROYAL SOCIETY OF CHEMISTRY

www.rsc.org/pccp

Early Regimes of Water Capillary Flow in Slit Silica Nanochannels

Elton Oyarzua,[†] Jens H. Walther,[‡,¶] Andrés Mejía,[†] and Harvey A. Zambrano[*,†]

Department of Chemical Engineering, Universidad de Concepcion, Concepcion, Chile, Department of Mechanical Engineering, Technical University of Denmark, DK-2800, Kgs. Lyngby, Denmark, and Computational Science and Engineering Laboratory, ETH Zurich, CH-8092, Switzerland

E-mail: harveyzambrano@udec.cl
Phone: +56 (0)41 2201468

Abstract

Molecular dynamics simulations are conducted to investigate the initial stages of spontaneous imbibition of water in slit silica nanochannels surrounded by air. An analysis is performed of the effects of nanoscopic confinement, initial conditions of liquid uptake and air pressurization on the dynamics of capillary filling. The results indicate that the nanoscale imbibition process is divided in three main flow regimes. An initial regime where the capillary force is balanced only by the inertial drag and characterized by a constant velocity and a plug flow profile. In this regime, the meniscus formation process plays a central role in the imbibition rate. Thereafter, a transitional regime takes place, in which, the force balance has significant contributions from both inertia and viscous friction. Subsequently, a regime, wherein viscous forces dominate the capillary force balance, is attained. Flow velocity profiles identify the passage from an inviscid flow to a developing Poiseuille flow. Gas density profiles ahead of the capillary front indicate a transient accumulation of air on the advancing meniscus. Furthermore, slower capillary filling rates com-
puted for higher air pressures, reveal a significant retarding effect of the gas displaced by the advancing meniscus.

Keywords

Capillary filling, nanofluidics, molecular dynamics, nano-channels, solid-liquid interfaces

Introduction

Nature has over million of years optimized nano-scale bio-machinery to work efficiently in an aqueous environment.[1,2] Therefore, a molecular level understanding of fluid transport is critical to pursue novel opportunities in biochemistry, drug delivery technology and medical diagnostic devices. Indeed, fabrication techniques have evolved dramatically over the past two decades,[3–6] allowing us to conceive integrated systems in length scales comparable to the size of intra-cellular structures,[5,7–9] opening the door to mimic the highly efficient natural fluidic processes in different technological areas.[10–13] Nevertheless, the study of flows confined inside nano-structures presents challenges to the application of macroscopic theories of fluids due to the fact that inherent to the nanoscale confinement, the extremely large surface to volume ratio, and the short time

---

[*]To whom correspondence should be addressed
[†]Universidad de Concepcion
[‡]Technical University of Denmark
[¶]ETH Zurich

and length scales dominate the fluid transport. Therefore, an important bottleneck for design and fabrication of integrated nano-devices arises from predicting the flows throughout nanoscopic conduits.

In nanofluidics, an important transport mechanism is capillary action.[14,15] The fundamentals of the current understanding of capillarity are based on the early 19th century contributions made by Young[16] and Laplace.[17] The Young-Laplace theory of capillarity relates the pressure difference across a curved interface (Laplace pressure) to the surface tension acting on the interface as a result of its curvature. On the dawn of the 20th century, the works carried out by Bell and Cameron[18] and later by Washburn[19] and Lucas,[20] found capillary filling to be square root dependent of time. The Lucas-Washburn (LW) equation relates the Laplace pressure across the capillary meniscus to the Hagen-Poiseuille equation for a fully developed viscous flow. Hence, the LW equation[19] describes the capillary filling assuming the no-slip boundary condition and considering the liquid penetration as being determined by a balance among the capillary force and the viscous drag force. For the water invasion of a slit channel with width much larger than the height, the LW equation results in:

$$l(t) = \sqrt{\frac{\gamma H \cos\theta}{3\mu}}\sqrt{t} \qquad (1)$$

where l is the imbibition length, t is time, H is the channel height, μ is the dynamic viscosity (for the SPC/E water used herein: $\mu = 0.729\,\mathrm{mPa\,s}$), γ is the surface tension (for SPC/E water: $\gamma = 0.072\,\mathrm{N/m}$), and θ is the static contact angle of the liquid on the channel wall. In this purely viscous flow model, the position of the meniscus relates with time as $l \propto \sqrt{t}$. Despite the fact that considerable effort has been devoted to develop more sophisticated models of capillarity,[21–29] it has been certainly possible, in many technological applications, to assume a scenario where LW equation predicts the capillary filling with sufficient accuracy. Nevertheless, in experiments of capillarity performed in sufficiently long nanoscale conduits,

the imbibition kinetics qualitatively follows the LW model.[30–36] However, the same experiments reported a slower filling rate than that predicted by the LW equation. In fact, during the last decade different explanations have been proposed for the observed reduction in the capillary filling speed. Therefore, Tas et al.[31] attributed the slower capillary rates to the electroviscous effect. Persson et al.[30] extended the results reported by Tas et al.[31] and concluded that other effects, different to the electroviscosity, also contribute to the observed deviations in the imbibition rates. In the same context, Mortensen and Kristensen[37] found that the contribution of the electroviscous effect to the apparent viscosity is less than $1\,\%$ therefore concluded that the electroviscous effect is not sufficiently strong to account for observed deviations. Subsequently, Thamdrup et al.[32] shown that the slower rates could be related to the formation of gas nanobubbles. Nevertheless, as pointed out by van Honschoten et al.[14] the Washburn model is derived for water imbibition without gas bubbles. Moreover, Chauvet et al.[38] found that slower capillary filling rates cannot be explained by enhanced viscous resistance due to nanobubbles. Specifically, Chauvet et al.[38] inferred that in sub $100\,\mathrm{nm}$ channels, the enhanced hydrodynamic resistance induced by the presence of nanobubbles is compensated by the effect of the reduced volume to fill induced by the same gas nanobubbles. An alternative explanation to the filling deviations was presented by Haneveld et al.[33] They proposed that water ordering near the channel walls due to strong liquid-surface interaction could be the origin of an interfacial region with enhanced viscosity which could explain the observed reduced capillary rates in nanochannels. The explanation proposed by Haneveld et al.[33] seems to correspond to the negative velocity slip length in silica pores reported by Gruener et al.[39] in experiments of water filling in networks of nanopores. Nevertheless, other detailed studies have not found such an interfacial layer with enhanced viscosity.[40–43] Furthermore, open questions remain about the role of line tension,[44,45] molecular roughness,[46,47] precursor films,[24,48] dynamic contact angle[26,28,49] and air displaced

by the advancing meniscus.[38,50] Therefore, a comprehensive explanation to the slower than expected capillary rates observed in the filling of nanochannels as compared to the LW equation predictions, remains an open question.[14,51]

The LW equation is an asymptotic model for long times of filling, when considering filling in short time and length scales, the LW model predicts an infinite imbibition velocity at $t = 0$. This singularity in the LW model has been attributed to the absence of the inertial drag related to the accelerating mass of fluid.[15,21,50,52–56] In 1923 Bosanquet[52] incorporated in a momentum balance equation the contributions of inertial drag and viscous resistance counteracting the capillary pressure. The Bosanquet equation, modified to describe the present capillary filling in a rectangular cross-section channel of width much greater than the height is:

$$l(t)^2 = \frac{2A_I^2}{B}\left[t - \frac{1}{B}\left(1 - \exp\left(-Bt\right)\right)\right] \quad (2)$$

with,

$$A_I = \sqrt{2\frac{\gamma\cos\theta}{\rho H}} \quad (3)$$

$$B = \frac{12\mu}{\rho H^2} \quad (4)$$

where ρ is the liquid density (here $\rho = 997\,\text{kg/m}^3$). The terms A_I and B represent the contributions to the capillary force balance from the inertial drag and from the viscous friction losses, respectively. In order to derive solutions to the momentum balance equation, Bosanquet assumed a particular scenario where the initial momentum of the liquid is zero. The derived solution depicts two cases. A visco-inertial regime for imbibition times sufficiently long, where the capillary filling can be described under the assumption of a developing viscous flow with a vanishing inertial drag effect $(A_I \to 0)$. In this case, the Bosanquet model gradually converges into the LW model. In the opposite limiting situation, where the viscous force is much weaker than the inertial drag and the capillary force, the Bosanquet solution of

the momentum balance equation gives:

$$l(t) = A_I t \quad (5)$$

where the A_I factor represents a constant initial velocity corresponding to the inertial term in the Bosanquet equation (Eq. (2)). Mathematically, the velocity A_I is a singular point of the Bosanquet equation, obtained by applying boundary conditions as limits on the imbibition velocity and the position of the capillary front. Certainly, by taking into account the inertial drag, the methodology used by Bosanquet effectively overcome the infinite velocity problem in the LW equation at $t = 0$. Nevertheless, it leaves open questions about the physical sense of the initial conditions at the beginning of the liquid uptake. Moreover, as pointed out by Kornev and Neimark[57] and Andrukh et al.,[58] Bosanquet did not consider important phenomena affecting the imbibition dynamics at early times. Indeed, the Bosanquet equation neglects the relation between the initial velocity (A_I) and the momentum associated to the liquid moving towards the capillary entrance. When a liquid approaches a hydrophilic solid, once it enters the range of action of intermolecular forces, the adhesion effect gives rise to a start up impulse which affects the initial velocity of the liquid invasion. Therefore, quantitatively, the Bosanquet model cannot describe the initial kinetics of the capillary filling.[56–58] Moreover, in nano-confinement, the capillary filling speeds are typically high,[54,55,59] therefore incorrect values of the velocity in the initial inviscid regime may result in significant deviations for predicting flow rates in short nano-slits.

Recently, the role of displaced gas on the capillary imbibition in closed-end[60–62] and open-end nanochannels,[38,50] has been addressed. In particular, Hultmark et al.[50] considered the role of viscous resistance from the displaced air on the kinetics of capillary filling, while Chauvet et al.[38] studied the effect on the imbibition rates of the transient pressurization of the air ahead of the capillary front.

In this study, we report molecular simulations performed to analyze the wetting kinetics in nano-confined fluids.[43,54,63–69] Providing

an atomistic description of the capillary filling process in its earliest time stage and during the subsequent transition towards a fully developed flow regime, our study allows a complete characterization of the kinetics of liquid imbibition in nanodevices. Moreover, since the time scale associated to the diffusion of air throughout nanochannels is much larger than the time scale associated to the advancing capillary front, we examine the effect of air ahead of the moving meniscus as it is displaced by the liquid filling a slit channel at different air pressures.

Simulation Details

To study the spontaneous capillary imbibition of water in an amorphous silica slit, a series of all-atoms MD simulations are conducted using the simulation package FASTTUBE.[66,70–72] We use the potentials previously developed for modeling silica, water and air.[73] In this force field, the potentials have been calibrated using dedicated criteria such as the contact angle of a water droplet on a silica surface ($\theta = 15°$), and the solubility of air in water at different pressures. The model is based on the simple point charge SPC/E model,[74] and molecular nitrogen and oxygen. The silica is described by the TTAMm model developed by Guissani and Guillot.[75] For details of the potential we refer the reader to Zambrano et al.[73] To create an amorphous silica channel, cristobalite cells are replicated to build two parallel crystalline slabs. An annealing procedure is implemented,[73,76] wherein, the two silica slabs are coupled to a Berendsen heat bath with a time constant of 0.1 ps. The cristobalite is heated to 3000 K keeping the temperature constant during 10 ps, subsequently, quenching the system from 3000 K to 300 K by imposing a cooling rate of 70 K/ps until the equilibrium state is reached.

The MD simulations are conducted to study the water imbibition in channels of different height ($H = 4$, 6, 8, and 10 nm) surrounded by an air atmosphere at 0, 5, 10, 20 and 250 bar. The system consists of two slabs of amorphous silica with size of 31.6 nm $\times$ 2.5 nm $\times$ 3.4 nm

representing the channel walls. The slabs are aligned parallel to the x-y plane, while the height (H) of the channel is defined along the z-axis cf. Figure 1. The simulations are conducted in a periodic orthorhombic box, the dimensions of the box are adjusted according to the size of each system and the corresponding air pressure to be reproduced. More details of the systems are listed in Table 1. In the simulations, using a time step of 2 fs, a water slab of 32000 molecules is coupled to a Berendsen thermostat[77] at 300 K during 0.5 ns; then, the thermostat is disconnected and the simulations are conducted in the microcanonical ensemble (NVE) until the system is equilibrated. Subsequently, the water slab is released from rest to move spontaneously towards the silica channels. In the systems with air, after the silica-water interactions are equilibrated, the air molecules are released in the NVT ensemble at 300 K during 0.6 ns, then the thermostat is disconnected and the simulations are conducted in the NVE ensemble for 25 ns to ensure proper equilibration of the water and the air molecules. Afterward, the water molecules are constrained to move toward the channel at low velocity (≈ 0.5 nm/ns) until the water enters the region of action of intermolecular forces. The low velocity is chosen to ensure that the imbibition kinetics is not affected by the imposed velocity. Moreover, in order to explore the effects of air on the later stage of imbibition, three systems consisting of a water slab with 55000 molecules filling slits with length of 50.6 nm are studied as listed in Table 1.

Results and discussion

In the present study, we conduct molecular dynamics (MD) simulations to investigate the spontaneous capillary imbibition of water in silica slit nanochannels as illustrated in Figure 1. The slit channels studied here have heights and lengths in the sub-100 nm range as listed in Table 1. The penetration lengths of water spontaneously filling slit channels are computed by tracking the instantaneous positions of the advancing capillary front. The axial velocity pro-

Table 1: List of the MD Simulations of Water Imbibition. H and L are the height and the length of the silica slit channels as illustrated in Figure 1. P is the corresponding gas pressure. The dimensions of the computational box are along the x, y and z directions, respectively.

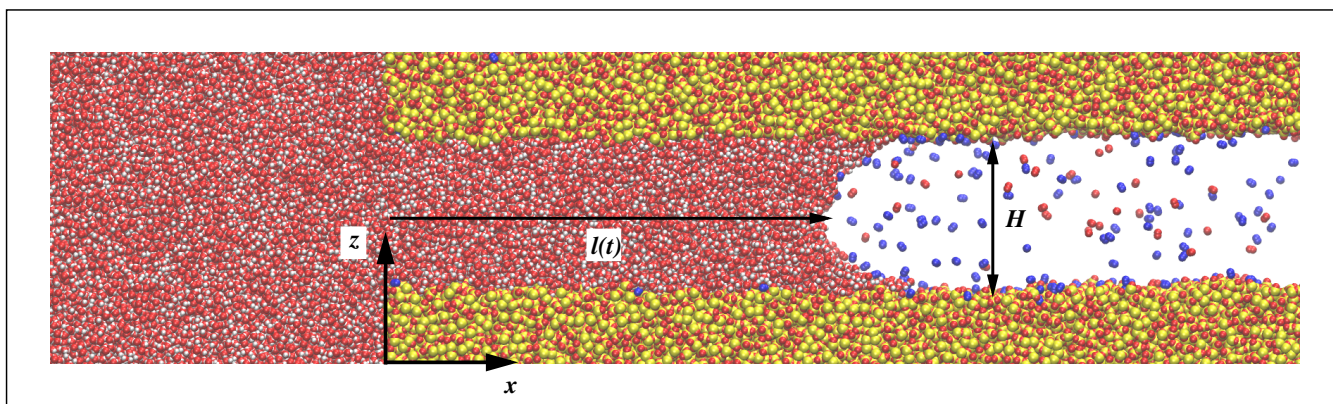| Case	H (nm)	L (nm)	P (bar)	box dimensions (nm)
1	4	31.6	0	$74 \times 2.5 \times 18.4$
2	6	31.6	0	$74 \times 2.5 \times 18.4$
3	6	31.6	5	$74 \times 2.5 \times 18.4$
4	6	31.6	10	$74 \times 2.5 \times 18.4$
5	8	31.6	0	$68 \times 2.5 \times 22.4$
6	8	31.6	5	$68 \times 2.5 \times 22.4$
7	8	31.6	10	$68 \times 2.5 \times 22.4$
8	10	31.6	0	$64 \times 2.5 \times 26.4$
9	10	31.6	5	$64 \times 2.5 \times 26.4$
10	10	31.6	10	$64 \times 2.5 \times 26.4$
11	6	50.6	0	$110 \times 2.5 \times 18.4$
12	6	50.6	20	$110 \times 2.5 \times 18.4$
13	6	50.6	250	$110 \times 2.5 \times 18.4$

Figure 1: Capillary filling of water in a nano-slit silica channel. H denotes the height of the channel and $l(t)$ the time dependent penetration length.

files are computed implementing a static binning procedure using a bin size of 0.2 nm along the z-axis. In order to estimate the effect on imbibition induced by gas molecules displaced by the advancing meniscus, density profiles of air ahead of the capillary front are computed using a dynamic binning with a reference frame attached to the center of the capillary meniscus. An example of the meniscus is shown in Figure 1. In Figure 2a, we plot the temporal evolution of the imbibition length as a function of time for a channel with of height of 10 nm. The dashed line represent a constant velocity regime of imbibition. The results indicate that at the beginning of the imbibition, the capillary front moves at constant velocity. Subsequently, at $t = 0.13$ ns the filling kinetics departs from being linear in time and follows a visco-inertial regime (Eq. (2)) depicted by the black solid line in Figure 2a. Furthermore, Figure 2b shows the capillary filling length as a function of time during the first 0.2 ns of the imbibition process for slit channels of 6, 8, and 10 nm. The time histories confirm that during the early time of capillarity, the progression of the meniscus position displays a linear dependence of time, which indicates a capillary flow with constant velocity for all the channels. The slopes of the linear fits represent velocities of ca. 52, 31, and 20 nm/ns for slits of 6, 8, and 10 nm, respectively. The de-
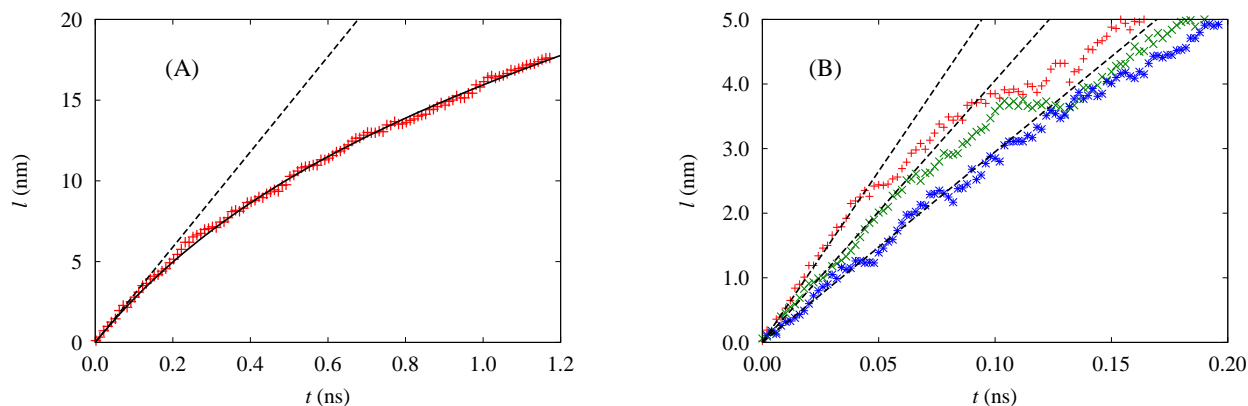
Figure 2: Position of capillary front as a function of time. (A) The red points (+) depict the imbibition length as a function of t for a slit channels of 10 nm. The black dashed line are visual guides to indicate the $l(t) = A_I t$ regime and the black solid line depicts the visco-inertial filling regime. (B) The red (+), green (×) and blue (∗) points depict the imbibition length as a function of t for channels of 6, 8, and 10 nm, respectively. The dashed lines are visual guides indicating the linear least-squares fit to the constant velocity regime.

crease in velocity for increasing channel height is consistent with Eq. (3) and previous studies.[15,55,56,58] Moreover, the results indicate that the duration of the inviscid regime is height dependent. Therefore, the transition times (t_I), between the filling regimes, are 0.05, 0.07 and 0.13 ns for the channels of 6, 8, and 10 nm cf. Figure 2b.

Figure 3 shows the axial velocity profiles computed at different stages of the capillary filling in a slit channel of 6 nm. In order to compute the axial velocities, atomic trajectory data have been collected every 10 fs. The dashed black line depicts the flow velocity profile computed between $t = 0.010$ ns and $t = 0.045$ ns. The profile exhibits a plug shape which indicates that during the corresponding period the flow is inviscid. Hence during this period the capillary force is counteracted exclusively by inertial effects. Moreover, to confirm the regime during the early time of capillarity is primarily inviscid, we estimate the deviation from a fully developed Poiseuille flow by following a similar procedure to that reported by Choi et al.[78] We solve the Navier-Stokes equations for a slit channel with height of 6 nm, where the capillary flow is driven exclusively by the Laplace pres-
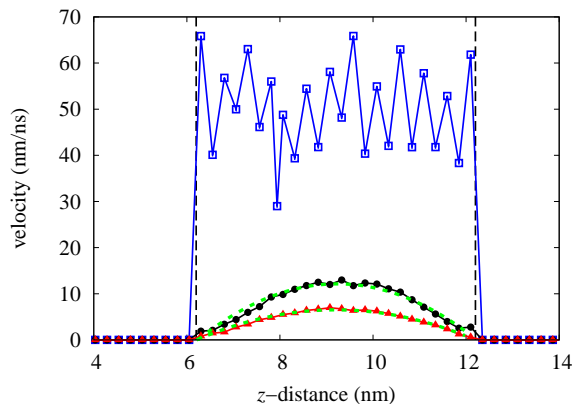

Figure 3: Axial velocity profiles for a slit channel with height of 6 nm. The reference position ($z = 0$) is located at the boundary of the computational domain. The profiles are computing extracting trajectories every 10 fs. The vertical dashed black lines represent the position of the channel walls. The solid blue (□), black (●), and red (△) lines are velocity profiles sampled at $t \in [0.010, 0.045]$ ns, $t \in [2.200, 3.200]$ ns, and $t \in [4.100, 5.000]$ ns, respectively. The dotted green lines depict the fit to a parabolic flow profile.

sure. Assuming that the resulting volumetric flow rate includes contributions from a viscous Poiseuille flow with parabolic profile and from an inviscid flow with plug like profile, we obtain

$$Q = \frac{wH^3}{12\mu}\frac{\Delta P}{l(t)} + Hwv_{wall} \qquad (6)$$

with

$$\Delta P = \frac{2\gamma\cos\theta}{\rho H} \qquad (7)$$

where, w is the width of the channel, ΔP is the Laplace pressure, θ is the instantaneous contact angle, and v_{wall} is the slip velocity at the wall. Rearranging Eq. (6) with Q, θ and $l(t)$ computed from the MD results of the 6 nm channel, we obtain a flow velocity at the channel wall of $v_{wall} = 44$ nm/ns. This high flow velocity at the wall is consistent with the velocity observed in Figure 3 at early times of 52 nm/ns. As found in previous investigations,[15,57,58] the magnitude of the initial constant velocities of capillarity computed here, do not correspond quantitatively to the velocities predicted by the Bosanquet inertial solution. Indeed, for a slit channel with height of 6 nm, the initial constant velocity predicted by the Bosanquet solution is $A_I = 150$ nm/ns, which is ca. 188% higher than the initial velocity computed in this study (Figure 3). In order to analyze the influence of the factors such as the pre-history of the wetting and the formation of the meniscus on the initial velocity of capillary imbibition we perform MD simulations of a slab moving towards the entrance of the slit channels with heights of 6 nm and 10 nm. In these simulations we impose different initial velocities. Specifically, the water slabs are released 1 nm away from the channel entrance at velocities between 0 and 40 nm/ns. Figure 4 shows the instantaneous position of the water free-surface during the pre-wetting period and, subsequently, the position of the capillary front during the beginning of the water uptake process for different imposed initial velocities: 0, 10, 20, 30, and 40 nm/ns, respectively. The results indicate that the velocity of imbibition during the inviscid regime of capillarity is not affected by the particular initial momentum. Moreover, we find that the
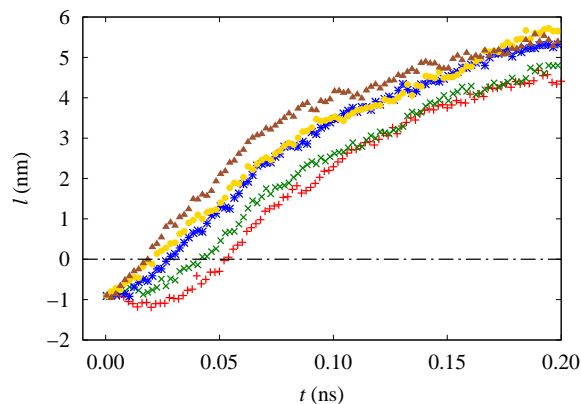

Figure 4: Pre-history of the capillary imbibition process for the channel of 6 nm. The red ($+$), green ($\times$), blue ($\ast$), yellow ($\bullet$) and brown ($\triangle$) points depict the temporal evolution of the position of the liquid-vacuum interface for imposed initial velocities of 0, 10, 20, 30, and 40 nm/ns respectively. The dashed black line indicates the position of the channel entrance. For all the imposed initial velocities, it could be observed a filling regime with constant velocity $l(t) = A_I t$ regime immediately after the water uptake.

capillary meniscus completes its formation at different distances depending of the particular channel height. For channels of 6 nm, we compute a dynamic contact angle of ca. 80° during the entire inviscid regime of imbibition (not shown). In fact, as we introduce the computed value of the initial dynamic contact angle in the Bosanquet inertial solution (Eq. (2)), the constant velocity, A_I, becomes equivalent to the corresponding velocity directly computed from the MD trajectories. It confirms that the process of formation of the capillary meniscus is part of the explanation to the quantitative deviations in the initial velocity of imbibition previously reported.[15,57,58] Nevertheless, we regard that more studies are required to determine the complex relation between the initial velocity of capillarity and coupled phenomena such as the hydrodynamic losses at the channel entrance,[69] the specific dynamic features of the imbibing flow, and the interfacial viscoelasticity[79] associated to the transfer of momentum at the beginning of the capillary uptake. During the later stages of the capillary filling, viscosity can no longer be neglected. Figure 2a shows that the inviscid constant velocity regime is followed by a subsequent period wherein the capillary filling kinetics departs from being linear in time. The velocity profile depicted by the solid black line in Figure 3 is computed in a channel with height of 6 nm. The axial velocities are averaged between $t = 2.2$ ns and $t = 3.2$ ns. The flow profile displays a significant velocity gradient in direction normal to the wall which confirms that viscous losses have to be taken into account. We infer that after the transition time, e.g., for a channel of 6 nm, $t_I = 0.05$ ns, the Laplace force driving the filling is balanced by a competition between inertial and viscous drags. We regard this stage of capillarity as the visco-inertial regime. Theoretical studies[53] of capillary filling have found that this visco-inertial stage following directly the purely inviscid-inertial regime, corresponds to the visco-inertial regime described by the Bosanquet equation[52] as the term $B \neq 0$ (Eq. (5)). In this work we compute the temporal position of the meniscus during the capillary filling of slit nanochannels and find good agree-

ment to the Bosanquet model (Eq. (2)). Indeed, Figure 2a and 5a show that the capillary filling kinetics follows the Bosanquet model for channels of 6 nm and 4 nm, respectively with a deviation of ca. 25 %. We attribute this deviation to the molecular roughness of the silica walls of the nanochannels. It should be noted that as the liquid imbibition evolves inside the channel, progressively the viscous flow losses will dominate the inertial drag. At the moment, when the viscous friction losses dominate the force due to the Laplace pressure, the Bosanquet filling regime converges into a regime dominated by the viscous friction drag where inertial effects can be neglected. Indeed, Figure 5 shows that the filling kinetics displays a $l(t) \propto \sqrt{t}$ after ca. 3.5 ns for a channel of 6 nm and after ca. 0.6 ns for a channel of 4 nm, respectively, which indicates that the capillary filling has reached the purely viscous regime. It should be noted that the filling kinetics for the channels of 4 and 6 nm deviates ca. 22 % from quantitative prediction using the LW equation (Eq. (1)).

We study systematically the influence of air on the imbibition kinetics of water in nanochannels by performing simulations of capillary filling at different air pressures. The density profiles shown in Figure 6 for the 6 nm channel subject to air pressures of 10 and 20 bar clearly demonstrate an accumulation of gas in front of the meniscus of ca. 4.0 kg/m^3 corresponding to an over-pressure of 3.5 bar. Similarly, the 10 nm channel subject to a gas pressure of 10 bar experience a gas accumulation of ca. 1.7 kg/m^3 and an over-pressure of 1.5 bar (Figure 6). The computed over-pressure values suggest that the accumulation of gas is size-dependent, higher over-pressures are computed for channels with smaller height. In order to extend the study of the effect of displaced air on the capillary filling rates, a simulation of a channel of 6 nm subject to an air pressure of 250 bar is conducted. In Figure 6, the density profile of air for the channel of 6 nm at 250 bar reveals an accumulation of gas in front of the meniscus of ca. 39.5 kg/m^3 corresponding to an over-pressure of 34 bar. Figure 5a show that the capillary filling kinetics qualitatively follows the Bosanquet model for a channels of 6 nm in the presence
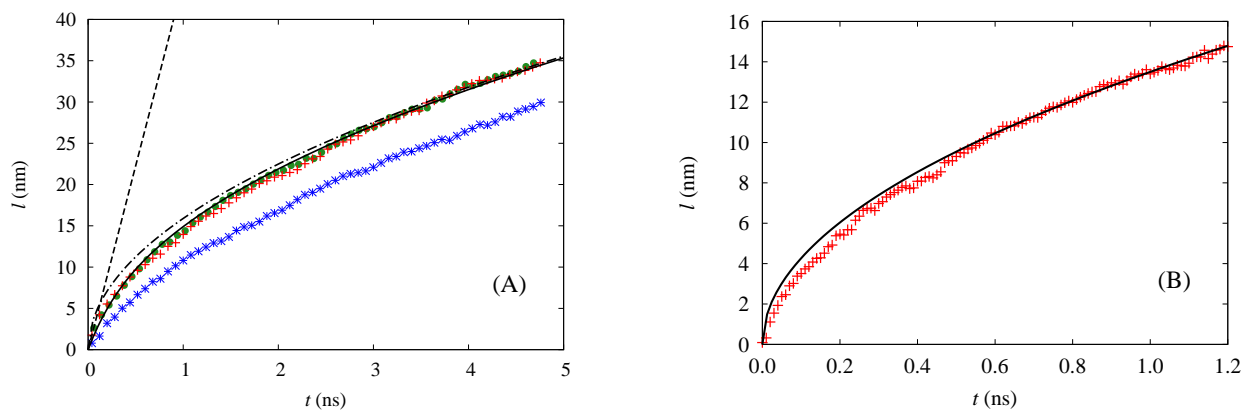
Figure 5: Imbibition length as a function of time. (A) The green (•), red (+) and blue (∗) points depict the position of the meniscus as a function of time for a channel of 6 nm in vacuum, at 20 and at 250 bar, respectively. The dashed lines correspond to a linear regression in the constant velocity regime. The solid and dashed-dotted black lines are a visual help to indicate the visco-inertial and LW ($l(t) \propto \sqrt{t}$) imbibition regimes. (B) The red (+) points show the position of the meniscus as a function of time for a channel of 4 nm in vacuum. The solid black line show the filling regime following $l(t) \propto \sqrt{t}$.

of air at 20 and 250 bar. Moreover, Figure 5a shows that the filling rate for the case of 250 bar deviates ca. 30 % from the filling rate computed at vacuum. It demostrates that air occupying nano-meter long slit channels does offer a significant mechanical resistance to the capillary penetration of the water. Furthermore, the results of the present study suggest that the accumulative effect of the gas viscous friction and the pressurization on the meniscus could be part of the explanation for the slower than expected capillary filling rates observed in experiments of long (> 100 nm) channels.[31–35]

Conclusion

In this study, we present an investigation of the early stage of capillarity in slit nanochannels in the nanoscale range. Performing all-atoms large scale MD simulations, we confirm that the spontaneous capillary filling of slit silica channels follows a purely inviscid flow regime with constant velocity during the very first stage of the imbibition. Subsequently, the capillary filling kinetics evolves in a developing flow where the capillary force is balanced by contributions

from inertia and viscous drag losses. As the filling length becomes sufficiently large, the inertial resisting effect on the imbibition dynamics, becomes negligible with regard to the viscous drag and a fully developed Poiseuille flow is attained.

Furthermore, the effect of the influence of air on the imbibition is systematically investigated. We predict a gas over-pressure in front of the advancing meniscus as the capillary action takes place. Moreover, our results indicate that in slit channels the air displaced by the imbibing water is found to have a significant effect on the capillary filling kinetics. In this study we provide an approach to extend the applicability of the Bosanquet model of capillarity to describe nanoscale imbibition of water. The approach consists of a modified Bosanquet equation with the initial constant velocity computed directly from atomistic simulations. The proposed model is suitable to describe the entire capillary filling process in nanoscopic slit channels in the presence of air.
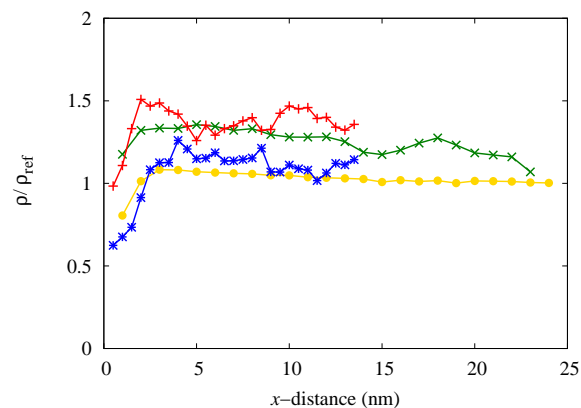
Figure 6: Transient accumulation of gas computed ahead of the capillary front. The reference densities (ρ_{ref}) are $9.8 \, \text{kg/m}^3$ for the channels of $6 \, \text{nm}$ and $10 \, \text{nm}$ at $10 \, \text{bar}$, $16 \, \text{kg/m}^3$ for the channel of $6 \, \text{nm}$ at $20 \, \text{bar}$ and $262 \, \text{kg/m}^3$ for the channel of $6 \, \text{nm}$ at $250 \, \text{bar}$, respectively. The green ($\times$) and yellow ($\bullet$) lines are the air densities for a channel with height of $6 \, \text{nm}$ at 20 and $250 \, \text{bar}$ as a function of the distance from the advancing meniscus. The red ($+$) and blue ($\ast$) lines depict the air density at $10 \, \text{bar}$ as a function of the distance from the advancing meniscus for channels with heights of $6 \, \text{nm}$ and $10 \, \text{nm}$, respectively.

References

1. Gravelle, S.; Joly, L.; Detcheverry, F.; Ybert, C.; Cottin-Bizonne, C.; Bocquet, L. Optimizing water permeability through the hourglass shape of aquaporins. *Proc. Natl. Acad. Sci. USA* **2013**, *110*, 16367.

2. Wang, J. Cargo-towing synthetic nanomachines: Towards active transport in microchip divices. *Lab on a Chip* **2012**, *12*, 1944–1950.

3. Gates, B. D.; Xu, Q.; Stewart, M.; Ryan, D.; Willson, C. G.; Whitesides, G. M. New approaches to nanofabrication: molding, printing, and other techniques. *Chemical Reviews.* **2005**, *105*, 1171–1196.

4. Biswas, A.; Bayer, I. S.; Biris, A. S.; Wang, T.; Dervishi, E.; Faupel, F. Advances in top down and bottom up surface nanofabrication: Techniques, applications and future prospects. *Adv. Coll. Interf. Sci.* **2012**, *170*, 2–27.

5. Kovarik, M. L.; Jacobson, S. C. Attoliterscale dispensing in nanofluidic channels. *Anal. Chem.* **2007**, *79*, 1655–1660.

6. Duan, H.; Berggren, K. K. Directed self-assembly at the $10 \, \text{nm}$ scale by using capillary force-induced nanocohesion. *Nano Lett.* **2010**, *10*, 3710–3716.

7. Sparreboom, W.; van den Berg, A.; Eijkel, J. C. T. Transport in nanofluidic systems: a review of theory and applications. *New J. Phys.* **2010**, *12*, 015004.

8. Whitby, M.; Quirke, N. Fluid flow in carbon nanotubes and nanopipes. *Nature Nanotechnol.* **2007**, *2*, 87–94.

9. Abgrall, P.; Nguyen, N. T. Nanofluidic devices and their applications. *Anal. Chem.* **2008**, *80*, 2326–2341.

10. Wei, D.; Bailey, M. J. A.; Andrew, P.; Ryhanen, T. Electrochemical biosensors at the nanoscale. *Lab on a Chip* **2009**, *9*, 2123–2131.

11. Vo-Dinh, T.; Cullum, B. M.; Stokes, D. L. Nanosensors and biochips: frontiers in biomolecular diagnostics. *SAB* **2001**, *74*, 2–11.

12. Balasubramanian, K. Challenges in the use of 1D nanostructures for on-chip biosensing and diagnostics: A review. *Biosens. Bioelect.* **2010**, *26*, 1195–1204.

13. Lee, J.; Laoui, T.; Karnik, R. Nanofluidic transport governed by the liquid/vapour interface. *Nature Nanotechnol.* **2014**, *9*, 1–7.

14. van Honschoten, J. W.; Brunets, N.; Tas, N. R. Capillarity at the nanoscale. *Chem. Soc. Rev.* **2010**, *39*, 1096–1114.

15. Quere, D. Inertial capillarity. *Europhys. Lett.* **1997**, *39*, 533–538.

16. Young, T. An essay on the cohesion of fluids. *Proc. Roy. Soc.* **1805**, *95*, 65–87.

17. Laplace, P. S. Traite de mecanique celeste. *Courcier Paris* **1805**, *2 Supplement au Livre X*, 349–498.

18. Bell, J. M.; Cameron, F. K. The flow of liquids through capillary spaces. *J. Phys. Chem.* **1906**, *10*, 658–674.

19. Washburn, E. W. The dynamics of capillary flow. *Phys. Rev.* **1921**, *17*, 273–283.

20. Lucas, R. Ueber das zeitgesetz des kapillaren aufstiegs von flssigkeiten. *Kolloid-Zeitschrift* **1918**, *23*, 15–22.

21. Szekely, J.; Neumann, A. W.; Chuang, Y. K. The rate of capillary penetration and the applicability of the washburn equation. *J. Coll. Interface Sci.* **1971**, *35*, 273–278.

22. Zhmud, B. V.; Tiberg, F.; Hallstensson, K. Dynamics of capillary rise. *J. Coll. Interface Sci.* **2000**, *228*, 263–269.

23. Xiao, Y.; Yang, F.; Pitchumani, R. A generalized analysis of capillary flows in channels. *J. Coll. Interface Sci.* **2006**, *298*, 880–888.

24. Chibbaro, S.; Biferale, L.; Diotallevi, F.; Succi, S.; Binder, K.; Dimitrov, D.; Milchev, A.; Girardo, S.; Pisignano, D. Evidence of thin-film precursors formation in hydrokinetic and atomistic simulations of nanochannel capillary filling. *Europhys. Lett.* **2008**, *84*, 44003.

25. Martic, G.; Gentner, F.; Seveno, D.; Coulon, D.; De Coninck, J.; Blake, T. D. A molecular dynamics simulation of capillary imbibition. *Langmuir* **2002**, *18*, 7971–7976.

26. Popescu, M. N.; Ralston, J.; Sedev, R. Capillary rise with velocity-dependent dynamic contact angle. *Langmuir* **2008**, *24*, 12710.

27. Joos, P.; van Remoortere, P.; Bracke, M. The kinetics of wetting in a capillary. *J. Coll. Interface Sci.* **1990**, *136*, 189–197.

28. Duvivier, D.; Blake, T. D.; De Coninck, J. Toward a predictive theory of wetting dynamics. *Langmuir* **2013**, *29*, 10132.

29. Dimitrov, D. I.; Milchev, A.; Binder, K. Forced imbibition a tool for separate determination of Laplace pressure and drag force in capillary filling experiments. *Phys. Chem. Chem. Phys.* **2008**, *10*, 1867–1869.

30. Persson, F.; Thamdrup, L. H.; Mikkelsen, M. B. L.; Jaarlgard, S. E.; Skafte-Pedersen, P.; Bruus, H.; Kristensen, A. Double thermal oxidation scheme for the fabrication of SiO2 nanochannels. *Nanotechnol.* **2007**, *18*, 1–4.

31. Tas, N. R.; Haneveld, J.; Jansen, H. V.; Elwenspoek, M.; van den Berg, A. Capillary filling speed of water in nanochannels. *Appl. Phys. Lett.* **2004**, *85*, 3274–3276.

32. Thamdrup, L. H.; Persson, F.; Bruus, H.; Kristensen, A.; Flyvbjerg, H. Experimental investigation of bubble formation during capillary filling of SiO_2 nanoslits. *Appl. Phys. Lett.* **2007**, *91*, 163505.

33. Haneveld, J.; Tas, N.; Brunets, N.; Jansen, H.; Elwenspoek, M. Capillary filling of sub-10 nm nanochannels. *J. Appl. Phys.* **2008**, *104*, 014309.

34. Han, A.; Mondin, G.; Hegelbach, N. G.; de Rooij, N. F.; Staufer, U. Filling kinetics of liquids in nanochannels as narrow as 27 nm by capillary force. *J. Coll. Interface Sci.* **2006**, *293*, 151–157.

35. Yang, D.; Krasowska, M.; Priest, C.; Popescu, M. N.; Ralston, J. Dynamics of capillary-driven flow in open microchannels. *J. Phys. Chem. C* **2011**, *115*, 18761–18769.

36. Cheng, J. T.; Giordano, N. Fluid flow through nanometer-scale channels. *Phys. Rev. E* **2002**, *65*, 1–5.

37. Mortensen, N. A.; Kristensen, A. Electroviscous effects in capillary filling of nanochannels. *Appl. Phys. Lett.* **2008**, *92*, 1–3.

38. Chauvet, F.; Geoffroy, S.; Hamoumi, A.; Prat, M.; Joseph, P. Roles of gas in capillary filling of nanoslits. *Soft Matter* **2012**, *8*, 10738.

39. Gruener, S.; Hofmann, T.; Wallacher, D.; Kityk, A. V.; Huber, P. Capillary rise of water in hydrophilic nanopores. *Phys. Rev. E* **2009**, *79*, 1–4.

40. Israelachvili, J. N. Measurement of the viscosity of liquids in very thin films. *J. Coll. Interface Sci.* **1986**, *110*, 263–271.

41. Horn, R. G.; Smith, D. T.; Haller, W. Surface forces and viscosity of water measured between silica sheets. *Chem. Phys. Lett.* **1989**, *162*, 404–408.

42. Raviv, U.; Laurat, P.; Klein, J. Fluidity of water confined to subnanometre films. *Nature* **2001**, *413*, 51–54.

43. Zhang, H.; Hassanali, A. A.; Shin, Y. K.; Knight, C.; Singer, S. J. The water-amorphous silica interface: Analysis of the Stern layer and surface conduction. *J. Chem. Phys.* **2011**, *134*, 024705.

44. Duncan, D.; Li, D.; Gaydos, J.; Neumann, A. W. Correlation of line tension and solid-liquid interfacial tension from the measurement of drop size dependence of contact angles. *J. Coll. Interface Sci.* **1995**, *169*, 256–261.

45. Peng, H.; Birkett, G. R.; Nguyen, A. V. The impact of line tension on the contact angle of nanodroplets. *Mol. Sim.* **2014**, *40*, 934–941.

46. Quere, D. Wetting and roughness. *Annu. Rev. Mater. Res.* **2008**, *38*, 71–99.

47. Nakamura, Y.; Carlson, A.; Amberg, G.; Shiomi, J. Dynamic wetting at the nanoscale. *Phys. Rev. E* **2013**, *88*, 1–10.

48. Blake, T. D.; De Coninck, J. The influence of solid-liquid interactions on dynamic wetting. *Adv. Coll. Interf. Sci.* **2002**, *96*, 21–36.

49. Stroberg, W.; Keten, S.; Liu, W. K. Hydrodynamics of capillary imbibition under nanoconfinement. *Langmuir* **2012**, *28*, 14488–14495.

50. Hultmark, M.; Aristoff, J. M.; Stone, H. A. The influence of the gas phase on liquid imbibition in capillary tubes. *J. Fluid Mech.* **2011**, *678*, 600–606.

51. Rauscher, M.; Dietrich, S. Wetting phenomena in nanofluidics. *Annu. Rev. Mater. Res.* **2008**, *38*, 143–172.

52. Bosanquet, C. H. On the flow of liquids into capillary tubes. *Phil. Mag. Ser. 6* **1923**, *45*, 525–531.

53. Fries, N.; Dreyer, M. The transition from inertial to viscous flow in capillary rise. *J. Coll. Interface Sci.* **2008**, *327*, 125–128.

54. Supple, S.; Quirke, N. Rapid imbibition of fluids in carbon nanotubes. *Phys. Rev. Lett.* **2003**, *90*, 214501.

55. Das, S.; Waghmare, P. R.; Mitra, S. K. Early regimes of capillary filling. *Phys. Rev. E* **2012**, *86*, 067301.

56. Ridgway, C. J.; Gane, P. A. C.; Schoelkopf, J. Effect of capillary element aspect ratio on the dynamic imbibition within porous networks. *J. Coll. Interface Sci.* **2002**, *252*, 373–382.

57. Kornev, K. G.; Neimark, A. V. Spontaneous penetration of liquids into capillaries and porous membranes revisited. *J. Coll. Interface Sci.* **2001**, *235*, 101–113.

58. Andrukh, T.; Monaenkova, D.; Rubin, B.; Lee, W.-K.; Kornev, K. G. Meniscus formation in a capillary and the role of contact line friction. *Soft Matter* **2014**, *10*, 609–615.

59. Joly, L. Capillary filling with giant liquid/solid slip: Dynamics of water uptake by carbon nanotubes. *J. Chem. Phys.* **2011**, *135*, 214705.

60. Phan, V. N.; Nguyen, N.-T.; Yang, C.; Joseph, P.; Djeghlaf, L.; Bourrier, D.; Gue, A.-M. Capillary filling in closed end nanochannels. *Langmuir* **2010**, *26*, 13251–13255.

61. Bakli, C.; Chakraborty, S. Effect of entrapped phase on the filling characteristics of closed end nanopores. *Soft Matter* **2015**, *11*, 161–168.

62. Schneider, D.; Valiullin, R.; Monson, P. A. Filling dynamics of closed end nanocapillaries. *Langmuir* **2014**, *30*, 1290–1294.

63. Qiao, R.; Aluru, N. R. Charge inversion and flow reversal in a nanochannel electro-osmotic flow. *Phys. Rev. Lett.* **2004**, *92*, 1–4.

64. Qiao, R.; Aluru, N. R. Surface-charge-induced asymmetric electrokinetic transport in confined silicon nanochannels. *Appl. Phys. Lett.* **2005**, *86*, 1–3.

65. Lorenz, C. D.; Crozier, P. S.; Anderson, J. A.; Travesset, A. Molecular dynamics of ionic transport and electrokinetic effects in realistic silica channels. *J. Phys. Chem. C* **2008**, *112*, 10222–10232.

66. Zambrano, H. A.; Walther, J. H.; Koumoutsakos, P.; Sbalzarini, I. F. Thermophoretic motion of water nanodroplets confined inside carbon nanotubes. *Nano Lett.* **2009**, *9*, 66–71.

67. Argyris, D.; Cole, D. R.; Striolo, A. Ion-specific effects under confinement: The role of interfacial water. *ACS Nano.* **2010**, *4*, 2035–2042.

68. Walther, J. H.; Ritos, K.; Cruz-Chu, E. R.; Megaridis, C. M.; Koumoutsakos, P. Barrier to superfast water transport in carbon nanotube membranes. *Nano Lett.* **2013**, *13*, 1910–1914.

69. Popadić, A.; Walther, J. H.; Koumoutsakos, P.; Praprotnik, M. Continuum simulations of water flow in carbon nanotube membranes. *New J. Phys.* **2014**, *16*, 082001.

70. Walther, J. H.; Jaffe, R.; Halicioglu, T.; Koumoutsakos, P. Carbon nanotubes in water: Structural characteristics and energetics. *J. Phys. Chem. B* **2001**, *105*, 9980–9987.

71. Werder, T.; Walther, J. H.; Jaffe, R. L.; Halicioglu, T.; Koumoutsakos, P. On the water-graphite interaction for use in MD simulations of graphite and carbon nanotubes. *J. Phys. Chem. B* **2003**, *107*, 1345–1352.

72. Walther, J. H.; Werder, T.; Jaffe, R. L.; Gonnet, P.; Bergdorf, M.; Zimmerli, U.; Koumoutsakos, P. Water-carbon interactions III: The influence of surface and fluid impurities. *Phys. Chem. Chem. Phys.* **2004**, *6*, 1988–1995.

73. Zambrano, H. A.; Walther, J. H.; Jaffe, R. L. Molecular dynamics simulations of water on a hydrophilic silica surface at high air pressures. *J. Mol. Liq.* **2014**, *198*, 107–113.

74. Berendsen, H. J. C.; Grigera, J. R.; Straatsma, T. P. The missing term in effective pair potentials. *J. Phys. Chem.* **1987**, *91*, 6269–6271.

75. Guissani, Y.; Guillot, B. A numerical investigation of the liquid-vapor coexistence Curve of Silica. *J. Chem. Phys.* **1996**, *104*, 7633–7644.

76. Huff, N. T.; Demiralp, E.; Cagin, T.; Goddard, W. A. Factors affecting molecular dynamics simulated vitreous silica structures. *J. Non-Crystal. Solids* **1999**, *253*, 133–142.

77. Berendsen, H. J. C.; Postma, J. P. M.; van Gunsteren, W. F.; DiNola, A.; Haak, J. R. Molecular dynamics with coupling to an external bath. *J. Chem. Phys.* **1984**, *81*, 3684–3684.

78. Choi, C.-H.; Westin, J. A.; Breuer, K. S. Apparent slip flows in hydrophilic and hydrophobic microchannels. *Phys. Fluids* **2003**, *15*, 2897–2902.

79. Kornev, K. G.; Neimark, A. V. Modeling of spontaneous penetration of viscoelastic fluids and biofluids into capillaries. *J. Coll. Interface Sci.* **2003**, *262*, 253–262.